
Article:
Nagy, B., Igneczi, A. orcid.org/0000-0003-1529-8383, Kovács, J. et al. (2 more authors) (2019) Shallow ground temperature measurements on the highest volcano of the Earth, the Mt. Ojos del Salado, Arid Andes, Chile. Permafrost and Periglacial Processes, 30 (1). pp. 3-18. ISSN 1045-6740

https://doi.org/10.1002/ppp.1989

Shallow ground temperature measurements on the highest volcano of the Earth, the Mt. Ojos del Salado, Arid Andes, Chile

Balázs Nagy[1], Ádám Ignéczi[2*], József Kovács[3], Zoltán Szalai[4], László Mari[1]

1: Department of Physical Geography, Eötvös University, Budapest, Hungary

2: Department of Geography, University of Sheffield, Sheffield, United Kingdom

3: Department of Physical and Applied Geology, Eötvös University, Budapest, Hungary

4: Department of Environmental and Landscape Geography, Eötvös University, Budapest, Hungary / Geographical Institute, MTA Research Centre for Astronomy and Earth Sciences, Budapest, Hungary

*: Corresponding author. e-mail: aigneczi1@sheffield.ac.uk

Abstract

The Mt. Ojos del Salado (6893 m a.s.l.) is situated within the Andean Arid Diagonal, on the Chilean-Argentinean border. Due to the extremely arid climate, surface ice is not widespread on the Mt. Ojos del Salado and at similar high altitude massifs in the region, though ice-bearing permafrost might be present. However, the thermal regime of the ground is relatively unknown in the region, especially outside of rock glaciers at high elevations north of 30°S. To study ground thermal regimes, in-situ shallow ground temperature and snow coverage from satellite imagery have been surveyed for four years (2012-2016) at six sites between the elevations of 4200-6893 m a.s.l. on the Mt. Ojos del Salado (27°07′S, 68°32′W). According to the ground temperature and snow coverage data at the six monitoring sites, the presence of permafrost is unlikely below 4550 m a.s.l. but likely above 5250 m a.s.l. on the Mt. Ojos del Salado. It was also observed that the active layer becomes extremely thin around 6750 m a.s.l.

Keywords:

Andes, ground temperature, permafrost, active layer, ground ice, aeolian processes

1. Introduction

The Puna de Atacama between 28°S - 22°S in Chile/Argentina has the highest theoretical equilibrium-line altitude (ELA) – at around 7000 m a.s.l. – on the Earth due to the extremely dry climate.[1,2] The regional ELA is just above the summit of the Mt. Ojos del Salado (27°07′S, 68°32′W, 6893 m a.s.l.), thus glaciers are rare on the mountain.[3,4] Although, perennial firn patches and small glaciers could be found in topographically sheltered positions,[2,5-8] the Mt. Ojos del Salado is the highest mountain on the Earth without significant ice coverage. However, ground ice could be present in the permafrost which is assumed to occur above 4000-5600 m a.s.l. in the Puna de Atacama, based on periglacial landform surveys and permafrost modelling.[9-11] This suggestion is supported by the presence of small transient lakes far from perennial firn patches at 5900-6000 m a.s.l. on the Mt. Ojos del Salado,[12] though evidence about the real volume of ground ice in the region is not available.

Despite recent advancements and the strong demand for detailed investigations,[13-15] there is still a considerable uncertainty about the distribution of permafrost and ground ice in the extremely arid zone of the Andes, north of 27°S. Systematic remote sensing based periglacial landform – most notably rock glacier – surveys have focused on areas south of 27°S.[14-22] Only a handful of such studies are available from the more arid northern region.[23-26] Well documented in-situ measurements of periglacial processes were focused on even more southerly areas – within the semiarid zone of the Andes – e.g. the Central Andes around 33.5°S,[27,28] and the Norte Chico around 30°S.[29-33] To date, only one in-situ study is available from the extremely arid zone of the Andes, providing four weeks of measurements about the daily heat transfer in the regolith at multiple sites between 27°S - 22.7°S.[34]

Long-term in-situ measurements of periglacial processes north of 30°S are still missing and permafrost outside of rock glaciers has remained largely unexplored.[13,15] Hence, we initiated a long-term monitoring programme in 2012 on the Chilean side of the Mt. Ojos del Salado, to constrain our knowledge about the thermal conditions of the ground at debris surfaces (excluding rock glaciers) by using shallow depth in-situ temperature loggers and satellite derived snow coverage data. Based on these datasets, we also provide preliminary suggestions about the potential presence of ground ice. In addition, sedimentological characteristics and the local geomorphology were assessed based on regolith samples and field observations at our study sites.

2. Study sites

The Puna de Atacama within the Andean Arid Diagonal, extending from 5°S on the west coast to 50°S on the east coast of South America and crossing the Andes at around 27°S - 30°S,[35-37] is one of the most extreme environments on the Earth due to its aridity, high altitude and strong winds.[38] This high altitude plateau – adjacent to the hyper-arid Atacama Desert – has a mean elevation of 4000 m a.s.l. and volcanoes reaching elevations well above 6000 m a.s.l. One of them is the 6893 m a.s.l. high dormant volcano complex,[39] the Mt. Ojos del Salado which is the highest volcano on the Earth (Fig. 1).

Six study sites were selected at different altitudes in the vicinity of the Mt. Ojos del Salado and on the volcano itself (Fig. 1, Table 1). Our lowest study site at the altitude of 4200 m a.s.l. was chosen to coincide with the lowest altitude where the presence of permafrost has been suggested by the literature.[10,11,40] Five more study sites were chosen at subsequently higher elevations up until the summit of the Mt. Ojos del Salado at 6893 m a.s.l. (Fig. 1, Table 1). The sample sites, with the exception of Laguna Negro Francisco, were delineated along the mountaineering route to the summit of the Mt. Ojos del Salado to ensure a relatively good accessibility. In order to minimise local effects that could bias our outcomes,[41-44] sample sites were chosen on relatively flat areas covered by debris (Table 1, Fig. 1), as far as possible from cliff faces, local topographical depressions – which are preferential sites for snow accumulation – and perennial snow patches.

3. Materials and methods

3.1. Ground temperature measurements and analyses

HOBO Pro v2 loggers (operation range: -40°C - 70°C, accuracy: ±0.21°C) were installed at multiple depths (10, 20, 35, 60 cm), which vary depending on the study site (Table 1), in shallow boreholes dug into the debris and covered with local ground material. Shallow ground temperatures were registered hourly by these loggers during our data acquisition periods between February 2012 and February 2016, the exact time intervals vary depending on the study site (Table 1). Daily mean ground temperatures (DMGT) were calculated by taking the mean of the hourly temperature measurements for each calendar day. Daily ground temperature variations (DGTV) were calculated by calculating the difference between the maximal and minimal temperature measurements of each calendar day. These calculations were carried out for the full data acquisition period of every temperature logger (Table 1). Annual Mean Ground Temperatures (AMGT) were calculated by taking the average of 365

DMGTs starting on 23 Feb 2012, which is the earliest initial installation date of the temperature loggers.

The presence of the permafrost, ground with temperatures below 0°C for at least two consecutive years,[45] could be deduced directly from our temperature record. However, this is only possible where the permafrost table – i.e. the upper boundary surface of permafrost[45] – is above the deepest temperature logger. As the loggers were buried at relatively shallow depths (Table 1), direct observations are restricted. Thus, the seasonal evolution of the near surface ground temperature have also been investigated. If the snow layer is thick enough to insulate the ground, temperatures become stable with small diurnal variations during winter. These winter equilibrium temperatures – measured near to the ground surface – are often used to infer the presence of permafrost in regions where the snow layer is thicker than about 0.8-1 m.[43-45] Furthermore, if water and ice is present in the ground, the latent heat of fusion causes the temperatures to persist close to 0°C with small diurnal variations (i.e. zero-curtain periods) during spring/autumn.[45,46] To aid the detection of these potential phenomena a time-frequency decomposition of the measured temperature signal was carried out by Morlet wavelet transformation (Eq. 1)

$$W_n(s) = \sum_{n=0}^{n} X_{n'} \Psi^* \left\lfloor \frac{(n' - n)\delta t}{s} \right\rfloor \quad \text{Eq. 1}$$

where the '*' represents the complex conjugate, 'X_n' the original data stream, 's' the scale, Ψ the wavelet function, and 'δ' the degree of resolution. This analysis is suitable to provide localized information – on the time domain – about the strength of certain frequencies in the signal,[47-50] such as the strength of daily periodicity in our temperature record. Firstly, it is recommended to remove large-scale trends from the signal, since they may hinder the estimation of small-scale periodicity. Thus, a centred 24 hour moving average was subtracted from the measured hourly temperature signal (Fig. 2). Then, the Morlet wavelet transformation was applied on the residuals in R using the dplR 1.6.4. package (Fig. 2).

In order to determine whether the peaks in our wavelet power spectra are significant – i.e. the strength of the measured temperature periodicity at a certain frequency and time differ significantly from an appropriate background noise – the wavelet transforms of our temperature records were compared with the corresponding theoretical red-noise Fourier spectra, which are calculated according to Torrence and Compo.[49] On average, the local wavelet power spectrum is identical to the theoretical Fourier spectrum,[49] which is χ_2^2 distributed as smoothing has not been applied.[49] Thus, the 0.95 confidence contours could be calculated[49] for our wavelet transforms (Fig 2). Temperature periodicity is considered

significant – at the 0.05 level – within these contours. Zero curtains have been delineated where the daily temperature periodicity is not significant and the raw hourly temperature is within -0.5°C and +0.5°C (Fig. 2).

3.2. Snow coverage survey

In order to account for its thermal effects, snow coverage was surveyed at our study sites for the period of ground temperature measurements – between February 2012 and February 2016 – by the visual interpretation of Landsat 7 Enhanced Thematic Mapper (ETM+) and Landsat 8 Operational Land Imager (OLI) Level 1 calibrated data (spatial resolution: 30 m) acquired from the U.S. Geological Survey. RGB combinations of 321, 453, and 543 of Landsat 7 ETM+ bands and RGB combinations of 432, 564, and 654 of Landsat 8 OLI bands were used for the visual interpretations. Three categories were separated: snow free, partial and full snow coverage.

The Moderate Resolution Imaging Spectroradiometer (MODIS) daily global Normalized Difference Snow Index (NDSI) version 6 product (spatial resolution: 500 m),[51,52] from both the Terra and Aqua satellites, has also been used to survey the snow coverage at our study sties. Firstly, the NDSI has been converted to fractional snow coverage (FSC) according to Riggs and Hall (Eq. 2.)[53]

$$\mathrm{FSC} = -0.01 + 1.45 \times \mathrm{NDSI} \qquad \text{Eq. 2}$$

The FSC was then sampled at our study sites and interpreted as snow free (FSC < 50%), partial (50% ≤ FSC < 90%) and full snow coverage (FSC ≥ 90%) to ensure compatibility with the Landsat derived snow coverage survey.

In total, 105 Landsat images were used, however, the number of snow coverage data points ranged from 96 to 105 due to cloud coverage. Thus, the actual mean temporal resolution – i.e. the average time between data points – of this snow coverage dataset is 14-15 days. Although the MODIS NDSI dataset has a daily nominal temporal resolution, the number of valid data points has ranged between 966-1233 due to cloud coverage and data quality issues. Hence, the actual mean temporal resolution is 1.27 and 1.41 days of the Terra and Aqua derived snow coverage datasets, respectively.

3.3. Measuring physical properties of the regolith and assessing local geomorphology

Regolith samples were collected in February, 2014 at the Atacama and Tejos Camps from the same depths as the temperature loggers (Table 1), by hitting metallic cylinders (diameter: 4 cm, length: 20 cm) into the walls of boreholes created near the loggers. The

containers were then closed airtight and transported to the laboratory where analyses were carried out in June-July 2014. The ratio of the coarse (d > 2 mm) and fine (d < 2 mm) grained fractions was determined by using Retsch sieve (d = 2 mm). Particle size distribution of the fine fraction was determined by Horiba Partica LA-950 V2 laser diffraction particle size analyzer, measuring in the range of 0.01 μm – 3 mm[54,55] with a refractive index of 1.54 and an imaginary part of 0.01.[56,57] Grain size classification was carried out according to the USDA (United States Department of Agriculture) texture classification scheme, modified by Konert and Vandenberghe.[54] Bulk density, overall porosity, ratio of macro- and micropores (Appendix 1), grain density of the fine and coarse fractions (Appendix 2), and hygroscopicity (Appendix 3) of the regolith samples were also measured.

In order to assess the local geomorphological context of these measurements, periglacial and aeolian landforms have been surveyed by field observations and Google Earth imagery in the vicinity of the Atacama and Tejos Camps. Instead of creating a comprehensive geomorphological map, our goal was simply to provide an inventory of the key non-volcanic landforms found in this area in order to guide future investigations.

3. Results

3.1. Snow coverage and ground temperature records in the vicinity of the Mt. Ojos del Salado

Winter snow coverage was observed at the Laguna Negro Francisco (4200 m a.s.l.), the Murray Lodge (4550 m a.s.l.) and the Atacama Camp (5260 m a.s.l.), especially in 2013 and 2015. However, instead of temperature stabilisation (i.e. the onset of a winter equilibrium temperature), only seasonal frost and high diurnal temperature variability was observed during each winter (Fig. 3, 4, 5). The depth of seasonal frost penetration is at least 35-60 cm at these sites, though this could be considerably larger according to the minimal DMGTs recorded by the deepest loggers: -4.4°C, -10°C and -7.9°C at the Negro Francisco (-60 cm, August 2015), Murray Lodge (-35 cm, July 2015), and Atacama Camp (-60 cm, July 2015) respectively (Table 2). Despite the lack of winter temperature stabilisation, relatively short periods of low diurnal temperature variability and temperatures close to 0°C (i.e. zero-curtain periods) were observed at the Atacama Camp (-35, -60 cm) during every spring and autumn, even without simultaneous snow coverage (Fig. 5, Table 2). Similar events were also observed at the Laguna Negro Francisco, the Murray Lodge and at shallower depths of the

Atacama Camp (-10 cm) but for only very short periods of time (Table 2) and mostly in relation to snow coverage periods, e.g. April 2015 (Fig. 3, 4, 5).

Similar to sites at lower elevations, at the Tejos Camp (5830 m a.s.l.) winter temperatures retained high diurnal variations at all depths, even during snow coverage events (Fig. 6). However, as opposed to the clear seasonal frost recorded by our loggers at smaller depths (-10 and -35 cm), temperatures only exceeded 0°C for brief periods at -60 cm (Fig. 6). Zero-curtains were observed to persist throughout each summer at -60 cm, and for around a month during each spring/autumn at -35 cm, regardless of surface snow coverage (Fig. 6). Regular zero-curtain events – during each spring/autumn – were also observed at -10 cm. However, these zero-curtains are less continuous and only last for a couple of weeks, except during snow coverage events e.g. February 2013 and April 2015 (Fig. 6).

At the Crater Edge (6750 m a.s.l.) and the Mt. Ojos del Salado summit (6893 m a.s.l.) diurnal temperature variations are high throughout our data acquisition period – except during some snow coverage events, e.g. February 2014 – and zero curtains were not observed (Fig. 7, 8). Although ground temperatures have risen above 0°C for a couple of hours during 11-30 days per year at smaller depths (i.e. -10 cm at the Crater Edge and the Mt. Ojos del Salado summit), positive temperatures were not measured at larger depths (i.e. -20 cm at the Crater Edge). Furthermore, maximal DMGTs remained well below 0°C at these sites and depths (Table 2). We also note that, the Landsat derived snow coverage dataset diverges significantly from the MODIS derived datasets at the Crater Edge (Fig. 7), despite the good general alignment elsewhere. This is attributed to the preferential accumulation of snow in topographical depressions situated in the close vicinity of the small ridge where the temperature loggers are buried at the Crater Edge (Fig. 1/H). This appears to dominate the Landsat derived dataset, while MODIS offers a more aggregated view about the general evolution of snow coverage around this site.

3.2. Landforms and physical properties of the regolith at the Atacama and Tejos Camps

In general, sediments are coarser at the Tejos Camp than at the Atacama Camp (Table 3). However, the proportion of coarse grains ($d > 2$ mm) is dependent on depth – with the lowest ratios at -35 cm – at both the Atacama and Tejos Camps (Table 3). At the Atacama Camp, particle size distribution curves of the fine fraction ($d < 2$ mm) are quite similar at different depths, though grains are generally larger at -60 cm (Fig. 9). At the Tejos Camp, the curves also align reasonably well, but at -35 cm the proportion of silt is particularly high (Fig. 9). The bulk density of the sediment samples is very low, especially at the Tejos Camp (Table

3). The grain density of the fine fraction has a distinctive vertical pattern at both study sites, with the lowest density found at -10 cm and the highest density at -35 cm (Table 3). These vertical density gradients are larger at the Tejos Camp than at the Atacama Camp.

Both sites have highly porous sediments, with porosity varying between 51-66% (v/v), but at the Tejos Camp porosity is considerably higher than at the Atacama Camp (Table 3). Although, macro-pores ($d > 10$ μm) are dominant at both sites, the proportion of capillaries ($d < 10$ μm) is significantly higher at the Tejos Camp than at the Atacama Camp (Table 3). Water adsorption capacity (i.e. hygroscopicity) of the sediment is weak at both sites and at all depths without significant differences, excluding -10 cm at the Atacama site (Table 3). Grains may adsorb a 200-1000 nm thick water film under wet conditions – RH96% – however when conditions are dry – RH 5.1% – the water film is less than 10-70 nm thick (Table 3).

In the vicinity of the Atacama and Tejos Camps clearly identifiable landforms related to cryoturbation, the movement and disturbance of soil caused by frost action,[45] were not found on the field. However, distinctive aeolian landforms were observed near to these sites. Above 5000 m a.s.l. boulders and bedrock outcrops exposed to the dominant direction of the wind show features of strong wind abrasion (Fig. 10/A), while blankets of coarse grained residual deposits – i.e. lag gravel pavements – were also found (Fig. 10/B). In addition to these erosional landforms, coarse grained dunes are also present on the lee-side slopes of ancient lava flows between the Atacama and Tejos Camps (Fig. 10/C). However, the most striking landforms found near these sites are gravel-mantled megaripples[38,58] around 5000-5500 m a.s.l. (Fig. 10/D). The wavelength and amplitude of the megaripples observed on the field are 15-20 m and 50-130 cm respectively, while the size of the megaripple fields range between 0.06-0.63 km^2 (Fig. 11). The base of the ripples is composed of light coloured, light-density pumice clasts – with a density of 0.8-1.1 g/cm^3 and a maximum size around 4-6 cm – while the top of the ripples is covered by dark coloured, dense volcanic litoclasts, with a density of 2.5-3 g/cm^3 and a maximum size around 1.8 cm (Fig. 10/E, F).

4. Discussion

4.1. Permafrost presence

Although the snow coverage is sporadic, a significant winter snowpack was present at our study sites in some years during the data acquisition period, e.g. 2013 and 2015. However, even during these periods, near surface ground temperatures have not stabilised and high

diurnal temperature variations dominated the record. This corresponds to the type-2 thermal regime described by Ishikawa[43] and is caused by the weak insulating effect of a thin and spatially discontinuous snowpack.[41-43] This is not surprising given the aridity of this region, which is confirmed by Espinoza et al.[59] who have reported an annual mean snow thickness below 5 cm for this region. These conditions hinder the development of winter equilibrium temperatures which are often used to infer the presence of permafrost from near surface ground temperature records.[43] Consequently, we can only confirm the presence of permafrost beyond doubt where the permafrost table is above our deepest temperature logger. Our outcomes correspond well to previous in-situ investigations from the Norte Chico (30°S), which also showed large daily ground temperature variability during winter due to insignificant snow coverage[29,30]. However, ground thermal regimes are different in the Central Andes (33.5°S) further to the south, where thicker snow coverage – due to more humid winters – enables the development of winter equilibrium temperatures, which were observed at a large number of sample sites by Apaloo et al.[28]

At the Laguna Negro Francisco, the Murray Lodge and the Atacama Camp, we have not detected permafrost directly, which could either mean that permafrost is not present or that the depth of the permafrost table larger than 35-60 cm at these sites. However, the distinctively positive AMGTs at all depths suggest that permafrost around the Laguna Negro Francisco and the Murray Lodge might be strongly restricted to preferential locations (Table 2). On the other hand, at the Atacama Camp AMGTs are just below 0°C at all depths (Table 2), which suggests that the presence of permafrost is more likely around this site compared to the Laguna Negro Francisco and the Murray Lodge. These findings align well with previous periglacial landform surveys suggesting 4150 m a.s.l. as a lowermost limit for permafrost occurrence in this region.[9,60] The modelling results of Gruber[11] also indicate that the presence of permafrost is less restricted to preferential locations at the Atacama Camp – which has a permafrost zonation index (PZI) of 0.54 – than at the Laguna Negro Francisco and the Murray Lodge, which are part of the PZI fringe of uncertainty (i.e. PZI = 0.01). However, PZIs are based on low resolution gridded annual mean air temperature data from the period of 1961-1990[11], and thus should be interpreted with caution against our outcomes.

At the Tejos Camp, our logger buried at -60 cm only recorded temperatures above 0°C for brief periods (Fig. 6). According to this, -60 cm is very close to the top of the possible permafrost table, thus we can infer the presence of permafrost at this site. This is in agreement with previous landform based suggestions for the region[9,60] and also with the modelling of Gruber[11] who reported a PZI of 0.94 at the Tejos Camp, suggesting that permafrost will occur

in most conditions around this site. As the thawing is already underway and the active layer is only about 60 cm thick, the area around the Tejos Camp (5830 m a.s.l.) could be particularly vulnerable to further atmospheric warming. At the Crater Edge and the Mt. Ojos del Salado summit hourly temperatures recorded by our loggers buried at -10 cm, only occasionally exceed 0°C. Therefore, we can infer the presence of permafrost at these sites, and suggest that the active layer is only slightly thicker than 10 cm.

4.2. The potential presence of liquid water and ice in the ground

Zero curtains – i.e. the persistence of ground temperatures close to 0°C accompanied by low diurnal temperature variations – usually indicate freezing-thawing in wet sediments.[46,61,62] At our temperature loggers this moisture could originate from melting snowpack, thawing ground ice and throughflow, i.e. water percolating laterally through the ground e.g. from melting perennial firn patches nearby. Although it is not possible to fully control for these potential moistures sources, we aim to reduce the chance of throughflow affecting our temperature records by burying the loggers at shallow depths on local topographical highs as far as possible from perennial firn patches. Also, we have surveyed the snow coverage at our study sites using multiple data sources in order to control for this potential moisture source as well. Consequently, we can provide suggestions about the potential sources of moisture causing the observed zero curtains on our temperature records.

At the Laguna Negro Francisco, the Murray Lodge and also at shallow depths of the Atacama Camp (-10 cm) short duration zero curtains were observed (Table 2) when snow coverage was present (Fig. 3, 4, 5). Therefore, we suggest that the primary source of the moisture causing these events is the melting snowpack. The most notable example corresponds to a large storm at the end of March 2015, causing the largest recorded floods in the region.[63] However, even this exceptional precipitation event[63] has not created a snowpack that could insulate the ground throughout the subsequent winter (Fig. 3, 4, 5). After May, 2015 daily ground temperature variations have gradually resumed, indicating a progressive decrease in snow thickness – especially at higher elevations (Fig. 5, 6) – probably due to the sublimation and wind redistribution of the snowpack.

However, at the Tejos Camp (-10, -35, -60 cm) and at larger depths of the Atacama Camp (-35, -60 cm), zero curtains appear to be less reliant on simultaneous snow coverage. At these sites and depths, zero curtains appear regularly during every spring/autumn – and in the case of the Tejos Camp (-60 cm) throughout most of the summer – both in the presence and absence of snow coverage (Fig. 5, 6). Therefore, we suggest that thawing ground ice – in

addition to melting snow – could be a potential source of moisture at these sites and depths. However, even at these two sites the upper layers of the regolith are relatively dry, which is demonstrated by the shorter duration of zero curtain periods (Table 2).

At the Crater Edge and the Mt. Ojos del Salado summit, ground temperature variability is very high throughout our data acquisition period (Fig. 7, 8). Furthermore, the potential for melting is extremely limited due to the low temperatures, which only occasionally exceed 0°C. Accordingly, zero curtains have not been observed (Table 2) and the potential for the presence of liquid water in the ground is very low. However, we can observe slightly dampened diurnal temperature variability during major snow coverage events, e.g. in February 2013 and in February 2014 (Fig. 7, 8), which we attribute to the weak insulating effect of the thin snowpack.

4.3. Sediments and geomorphological processes at the Atacama and Tejos Camps

Sediments are highly porous at both the Atacama and Tejos Camps with a high proportion of macro-pores (Table 3). This enhances infiltration at both sites which could partially explain the presence of dry upper layers, along with the high evaporation and sublimation.[64-66] However, the higher percentage of capillaries at the Tejos Camp (Table 3) indicates a higher water retention capacity compared to the Atacama Camp. Although the presence of ground ice is mostly controlled by thermal and hydrological characteristics, higher water retention capacity could limit the drying of the upper layers at the Tejos Camp. This is in agreement with our previous remarks suggesting the presence of ground ice below -10 cm at the Tejos Camp and below -35 cm at the Atacama Camp.

The observed vertical gradients in grain density (Table 3) – indicating preferential separation and migration of light particles to shallow depths within the top 35 cm – imply shallow cryoturbation at the Atacama and Tejos Camps. Vertical grain density gradients are higher at the Tejos Camp (Table 3), suggesting a higher degree of cryoturbation at this site. This is supported by our ground temperature records which imply that sediments at the Tejos Camp are less dry than at the Atacama Camp. However, even at the Tejos Camp patterned ground structures have not been found on levelled surfaces. Hence, we propose that cryoturbation is weak around our study sites due to the highly porous and dry sediments, limiting volumetric changes during freezing-thawing cycles.

Although periglacial landforms formed by cryoturbation were not found on the field around the Atacama and Tejos Camps (Fig. 10, 11), aeolian processes could be effective in the periglacial zone of the Mt. Ojos del Salado. This is due to the strong winds,[38,58,67] low

precipitation, high evaporation/sublimation,[37,66] and extremely sparse vegetation.[68] Hence, periglacial landforms could be overwritten by aeolian processes, creating a unique blend of periglacial and aeolian landscape. In fact, distinctive aeolian landforms have been found in the vicinity of the Atacama and Tejos Camps (Fig. 10), most notably gravel mantled megaripples between 5140-5480 m a.s.l. (Fig. 11). The dimensions of these megaripples are similar to the ones observed at lower elevations – around 4000 m a.s.l. – in the Argentinian Puna.[38,58]

5. Conclusions

Results presented here represent the highest altitude long-term in-situ data about ground thermal regimes in the South American Andes, as previously published short- and long-term ground temperature records are not available from higher altitudes than 5850 m a.s.l.[34] and 4700 m a.s.l.[29-30] respectively. According to our findings, the widespread presence of permafrost is unlikely below 4550 m a.s.l., but likely above 5250 m a.s.l. on the Mt. Ojos del Salado, at 27°S. Our ground temperature records also suggest that the regolith gets wet regularly – during every spring/autumn – in the elevation range of 5250-5850 m a.s.l. on the Mt. Ojos del Salado. Although more research is needed, we suggest ground ice could be a potential source of this moisture. These outcomes are consistent with previous research and fit nicely into the trend of increasing elevation of ice-bearing permafrost towards the north in the Arid Andes – consistent with increasing aridity – shown by previous in-situ and remote sensing investigations.

According to our results, sediments are relatively dry near to the surface and periglacial landform genesis is weak at our study sites. This, combined with the strong wind,[38] allows aeolian processes to overwrite periglacial landforms in the high altitude zone of the Mt. Ojos del Salado. In conclusion, we suggest that the zone between 5000 and 6000 m a.s.l. – just above the vast desert plateaus and below the steep taluses and remnant lava flows – is a distinct geomorphological zone on the Mt. Ojos del Salado, where landform genesis is mostly determined by the cold, dry and windy conditions. Further investigations in this region could yield interesting insights into the geomorphology of extremely cold, dry and windy periglacial environments, which could also serve as useful Mars analogues.[58,67]

Appendix 1: Density and porosity measurements

Undisturbed regolith cores of 100 cm^3 (V) were used to determine the bulk density (ρ_b), overall porosity (ϕ), and the ratio of macro- and micropores (ϕ_{ma}; ϕ_{mi}) at our study sites.[69,70] The cores were completely saturated with distilled water – using a vacuum-desiccator – then they were weighted (m_s). Subsequently the cores were weighted under field capacity (m_{fc}), and after drying them at 105°C (m_d). Using these measurements, the following calculations were carried out:

$$\rho_b = m_d \times V^{-1} \qquad \text{(Eq. 3)}$$

$$\phi = (m_s - m_d) \times V^{-1} \qquad \text{(Eq. 4)}$$

$$\phi_{ma} = (m_s - m_{fc}) \times V^{-1} \qquad \text{(Eq. 5)}$$

$$\phi_{mi} = (m_{fc} - m_d) \times V^{-1} \qquad \text{(Eq. 6)}$$

Appendix 2: Grain density measurements

After the separation of the coarse and fine fractions, a 25 cm^3 oven-dry sample from the coarse fraction was weighed (m_{gd}) then it was added to 50 cm^3 (V_0) distilled water at 24 C°. The suspension was gently boiled and slowly stirred for 30 minutes. Then it was cooled back to 24 C° and poured into a volumetric flask. The volume (V_s) of the suspension was recorded and the grain density (ρ_g) was calculated (Eq 7.).[71] The process was repeated for the fine fraction as well.

$$\rho_g = m_{gd} \times (V_s - V_0)^{-1} \qquad \text{(Eq. 7)}$$

Appendix 3: Hygroscopicity measurements

25 cm^3 oven-dry samples were weighed and put into dessicators with different relative humidity (RH) levels, which were provided by different concentrations of sulphuric acid: 70% (m/m) H_2SO_4 = RH 5.1%; 50% (m/m) H_2SO_4 = RH 36.9%; 24% (m/m) H_2SO_4 = RH 82.2%; 10% (m/m) H_2SO_4 = RH 96.2%.[72] Specimens were weighted after two days. The amount of adsorbed water was calculated by subtracting the oven-dry mass from the treated mass of the specimens. Thickness of the adsorbed water film – i.e. interfacial water – was calculated using the estimated surface area of the grains in the samples – inferred from the particle size distribution data – and the amount of adsorbed water.

Acknowledgements

This study was funded and supported by the Földgömb Foundation for Research Expeditions (Földgömb Expedíciós Kutatásért Alapítvány). A.I. was funded by a PhD grant from the Ice and Climate Research at Sheffield (ICERS). We also thank the support of the Embassy of Hungary in Chile and the Chilean-Hungarian Chamber of Commerce (Cámara Chileno-Húngara de Comercio). SRTM V.3.0 Global 1 Arc-Second, Landsat 7 ETM+, and Landsat 8 OLI data were retrieved from USGS Earth Explorer at http://earthexplorer.usgs.gov, courtesy of the NASA Land Processes Distributed Active Archive Center (LP DAAC). MODIS Terra/Aqua Snow Cover Daily L3 Global 500m Grid, Version 6 data were retrieved from NASA EarthData at https://earthdata.nasa.gov/, courtesy of NASA National Snow and Ice Data Center Distributed Active Archive Center (NSIDC DAAC). Google Earth imagery were retrieved on 16/Dec/2008, and viewed on 25/Oct/2016. We are grateful to the editor, Professor Julian Murton, the associate editor Dr Lukas Arenson and the two anonymous reviewers who have provided valuable suggestions regarding the manuscript.

References

1. Clapperton CM. The quaternary glaciation of Chile: a review. *Revista Chilena Hist Nat.* 1994;**67**:369-383.
2. Kull C, Grosjean M, Veit H. Modelling modern and Late Pleistocene glacio-climatological conditions in the North Chilean Andes (29-30° S). *Clim Change*. 2002;**52**(2):359-381. https://doi.org/10.1023/A:1013746917257
3. Cogley G (submitter), Miles E, De Angelis H, Moelg N, Sharp M, Paul F, Wyatt F (analyst(s)). GLIMS Glacier Database, Version 1. Boulder, CO, USA: NASA National Snow and Ice Data Center Distributed Active Archive Center; 2015. https://doi.org/10.7265/N5V9860210.7265/N5V98602. Accessed May 25, 2017
4. Cogley G (submitter), Sharp M, Miles E, Kienholz C, Wyatt F (analyst(s)). GLIMS Glacier Database, Version 1. Boulder, CO, USA: NASA National Snow and Ice Data Center Distributed Active Archive Center; 2015. https://doi.org/10.7265/N5V98602. Accessed May 25, 2017
5. Ammann C, Jenny B, Kammer K, Messerli B. Late Quaternary glacier response to humidity changes in the arid Andes of Chile (18–29 S). *Palaeogeogr Palaeoclimatol Palaeoecol*. 2001;**172**:313-326. https://doi.org/10.1016/S0031-0182(01)00306-6
6. Kull C, Grosjean M. Late Pleistocene climate conditions in the north Chilean Andes drawn from a climate-glacier model. *J Glaciol.* 2000;**46**(155):622-632. https://doi.org/10.3189/172756500781832611
7. Kull C, Hänni F, Grosjean M, Veit H. Evidence of an LGM cooling in NW-Argentina (22°S) derived from a glacier climate model. *Quat Int.*. 2003;**108**(1):3-11. https://doi.org/10.1016/S1040-6182(02)00190-8

8. Gspurning J, Lazar R, Sulzer W. Regional climate and snow/glacier distribution in Southern Upper Atacama (Ojos del Salado) – an integrated statistical, GIS and RS based approach. *Grazer Schriften Geogr Raumforschung*. 2006;**41**:59-70.

9. Trombotto D. Survey of cryogenic processes, periglacial forms and permafrost conditions in South America. *Revista do Instituto Geol São Paolo*. 2000;**21**(1/2):33-55. doi: https://doi.org/10.5935/0100-929X.20000004

10. Ahumada, AL. Periglacial phenomena in the high mountains of northwestern Argentina. *S Afr J Sci*. 2002;**98**:166-170.

11. Gruber S. Derivation and analysis of a high-resolution estimate of global permafrost zonation. *Cryosphere*. 2012;**6**:221–233. https://doi.org/10.5194/tc-6-221-2012

12. Aszalós JM, Krett G, Anda D, Márialigeti K, Nagy B, Borsodi AK. Diversity of extremophilic bacteria in the sediment of high-altitude lakes located in the mountain desert of Ojos del Salado volcano, Dry-Andes. *Extremophiles*. 2016;**20**(5):603-620. https://doi.org/10.1007/s00792-016-0849-3

13. Arenson LU, Jakob M. The Significance of Rock Glaciers in the Dry Andes – A Discussion of Azócar and Brenning (2010) and Brenning and Azócar (2010). *Permafr Periglac Process*. 2010;**21**:282-285. https://doi.org/10.1002/ppp.693

14. Janke JR, Bellisario AC, Ferrando FA. Classification of debris-covered glaciers and rock glaciers in the Andes of central Chile. *Geomorphology*. 2015;**241**:98-121. https://doi.org/10.1016/j.geomorph.2015.03.034

15. Azócar GF, Brenning A, Bodin X. Permafrost distribution modelling in the semi-arid Chilean Andes. *Cryosphere*. 2017;**11**:877–890. https://doi.org/10.5194/tc-11-877-2017

16. Rivera A, Brown F, Zenteno P, Bravo C. *Balance Glaciológico e Hídrico del Glaciar Nef, Campo de Hielo Norte, y Catastro de Glaciares de Algunas Cuencas de la Zona Central y Sur del País*. Santiago, Chile: Centro de Estudios Científicos (CECS); 2008

17. Favier V, Falvey M, Rabatel A, Praderio E, López D. Interpreting discrepancies between discharge and precipitation in high-altitude area of Chile's Norte Chico region (26-32°S). *Water Resour Res*. 2009;**45**:W02424. https://doi.org/10.1029/2008WR006802

18. Nicholson L, Marín J, Lopez D, et al. Glacier inventory of the upper Huasco valley, Norte Chico, Chile: glacier characteristics, glacier change and comparison with central Chile. *Ann. Glaciol*. 2009;**50**(53):111-118. https://doi.org/10.3189/172756410790595787

19. Azócar GF, Brenning A. Hydrological and Geomorphological Significance of Rock Glaciers in the Dry Andes, Chile (27°-33°S). *Permafr Periglac Process*. 2010;**21**:42-53. https://doi.org/10.1002/ppp.669

20. Brenning A, Azócar GF. Statistical Analysis of Topographic and Climate Controls and Multispectral Signatures of Rock Glaciers in the Dry Andes, Chile (27°-33°S). *Permafr Periglac Process*. 2010;**21**:54-66. https://doi.org/10.1002/ppp.670

21. Marangunic C, Pérez A, Peralta C, et al. *Catastro, Exploracíon y Estudio de Glaciares en Chile Central*. Santiago, Chile: Geoestudios LTDA; 2011

22. Perucca L, Angillieri MYE. Glaciers and rock glaciers' distribution at 28° SL, Dry Andes of Argentina, and some considerations about their hydrological significance. *Environ Earth Sci.* 2011;**64**:2079-2089. https://doi.org/10.1007/s12665-011-1030-z

23. Kammer K. Rock glaciers, Western Andes, Chile, Version 1. Boulder, CO, USA: NASA National Snow and Ice Data Center Distributed Active Archive Center; 1998. http://nsidc.org/data/ggd282. Accessed May 26, 2018.

24. Payne D. Climatic implications of rock glaciers in the arid Western Cordillera of the Central Andes. *Glacial Geol. Geomorphol*. 1998;rp03/1998

25. García A, Ulloa C, Medina C, Amigo G, Milana JP. Sustitución progresiva de geoformas criosféricas por la creciente aridez de la diagonal árida de América del Sur, Andes centrales entre 25°30'S y 29°30'S; Atacama, Chile. *XIV Congreso Geológico Chileno*. La Serena, Chile; 2015

26. Ulloa C, García A, Amigo G, Milana JP. Línea base de la Criósfera para la cuenca del Río Copiapó. *XIV Congreso Geológico Chileno*. La Serena, Chile; 2015

27. Bodin X, Rojas F, Brenning A. Status and evolution of the cryosphere and the Andes of Santiago (Chile, 33.5°S.). *Geomorphology*. 2010;**118**:453-464. https://doi.org/10.1016/j.geomorph.2010.02.016

28. Apaloo J, Brenning A, Bodin X. Interactions between Seasonal Snow Cover, Ground Surface Temperature and Topography. Permafr Periglac Process. 2012;**23**:277-291. https://doi.org/10.1002/ppp.1753

29. Schrott L. Global solar radiation, Soil Temperature and Permafrost in the Central Andes, Argentina: a Progress Report. *Permafr Periglac Process*. 1991;**2**:59-66. https://doi.org/10.1002/ppp.3430020110

30. Happoldt H, Schrott L. A Note on Ground Thermal Regimes and Global Solar Radiation at 4720 m a.s.l., High Andes of Argentina. *Permafr Periglac Process*. 1992;**3**:241-245.

31. Croce FA, Milana JP. Internal Structure and Behaviour of a Rock Glacier in the Arid Andes. *Permafr Periglac Process*. 2002;**13**:289-299. https://doi.org/10.1002/ppp.3430030312

32. Milana JP, Güell A. Diferencias mecánicas e hídricas del permafrost en glaciares de rocas glacigénicos y criogénicos, obtenidas de datos sísmicos en El Tapado, Chile. *Rev Asoc Geol Argent.* 2008;**63**(3):310-325.

33. Kinnard C, Monnier S, Abermann J, et al. *Caracterización y Monitoreo de Glaciares Rocosos en la Cuenca del Río Elqui y Balance de Masa del Glaciar Tapado*. Santiago, Chile: Centro de Estudios Avanzados end Zonas Áridas (CEAZA); 2012

34. Schröder H, Schmidt D. Morfología climática y morfogénesis del Volcán Llullaillaco (Chile/Argentina). *Norte Grande Geogr J*. 2000;**27**:69-92.

35. Messerli B, Grosjean M, Vuille M. Water availability, protected areas, and natural resources in the Andean desert Altiplano. *Mt Res Dev*. 1997;**17**(3):229-238. https://doi.org/10.2307/3673850

36. Vuille M, Ammann C. Regional snowfall patterns in the high, arid Andes. *Clim Change*. 1997;**36**:413-423. https://doi.org/10.1023/A:1005330802974

37. Houston J, Hartley AJ. The central Andean west-slope rainshadow and its potential contribution to the origin of hyper-aridity in the Atacama Desert. *Int J Climatol*. 2003;**23**:1453-1464. https://doi.org/10.1002/joc.938

38. Milana JP. Largest wind ripples on Earth?. *Geology*. 2009;**37**(4):343-346. https://doi.org/10.1130/G25382A.1

39. Moreno T, Gibbons W. *The Geology of Chile*. London, UK: The Geological Society; 2007.

40. Corte AE. Geocriología Argentina general y aplicada. *Revista Instituto Ciencias Geol*. 1982;**5**:87-120.

41. Harris SA, Brown RJE. Plateau mountain: a case study of alpine permafrost in the Canadian Rocky Mountains. *Proceedings 3rd International Conference on Permafrost*. Edmonton, Alberta, Canada; 1978:385-391.

42. Harris SA. Climatic relationships of permafrost zones in areas of low winter snow-cover. *Arctic*. 1981;**34**(1):64-70.

43. Ishikawa M. Thermal regimes at the snow-ground interface and their implications for permafrost investigation. *Geomorphology*. 2003;**52**:105-120. https://doi.org/10.1016/S0169-555X(02)00251-9

44. Brenning A, Gruber S, Hoelzle, M. Sampling and statistical analyses of BTS measurements. *Permafr Periglac Process*. 2005;**16**:383-393. https://doi.org/10.1002/ppp.541

45. van Everdingen R. *Multi-language glossary of permafrost and related ground-ice terms*. International Permafrost Association; 2005.

46. Outcalt IS, Nelson EN, Hinkel MK. The zero-curtain effect: heat and mass transfer across an isothermal region in freezing soil. *Water Resour Res.* 1990;**27**(7):1509-1516. https://doi.org/10.1029/WR026i007p01509

47. Daubechies I. The wavelet transform time-frequency localization and signal analysis. IEEE Trans Inf Theory. 1990;**36**:961–1004. https://doi.org/10.1109/18.57199

48. Meyers SD, Kelly BG, O'Brien JJ. An introduction to wavelet analysis in oceanography and meteorology: With application to the dispersion of Yanai waves. *Mon Wea Rev*. 1993;**121**:2858–2866.

49. Torrence C, Compo GP. A practical guide to wavelet analysis. *Bull Am Meteorol Soc*. 1998;**79**(1):61–78.

50. Kovács J, Hatvani IG, Korponai J, Kovács IS. Morlet wavelet and autocorrelation analysis of long–term data series of the Kis–Balaton water protection system (KBWPS). *Ecol Eng*. 2010;**36**(10):1469–1477. https://doi.org/10.1016/j.ecoleng.2010.06.028

51. Hall D, Riggs G. MODIS/Aqua Snow Cover Daily L3 Global 500m Grid, Version 6. Boulder, CO: NASA National Snow and Ice Data Center Distributed Active Archive Center; 2016. http://dx.doi.org/10.5067/MODIS/MYD10A1.006. Accessed November 22, 2017

52. Hall D, Riggs G. MODIS/Terra Snow Cover Daily L3 Global 500m Grid, Version 6. Boulder, CO: NASA National Snow and Ice Data Center Distributed Active Archive Center; 2016. http://dx.doi.org/10.5067/MODIS/MYD10A1.006. Accessed November 22, 2017

53. Riggs G, Hall D. *MODIS Snow Products Collection 6 User Guide*. https://nsidc.org/sites/nsidc.org/files/files/MODIS-snow-user-guide-C6.pdf. Published: December 11, 2015. Accessed November 22, 2017

54. Konert M, Vandenberghe J. Comparison of laser grain size analysis with pipette and sieve analysis: a solution for the underestimation of the clay fraction. *Sedimentology*. 1997;**44**:523–535.

55. HORIBA Instruments, Inc. *AN157 applications note. Refractive index selection for powder mixtures*. Irvine, CA: Horiba Instruments Inc.; 2008.

56. Eshel G, Levy GJ, Mingelgrin U, Singer MJ. Critical Evaluation of the Use of Laser Diffraction for Particle-Size Distribution Analysis. *Soil Sci Soc Am J*. 2004;**68**:736–743. https://doi.org/10.2136/sssaj2004.0736

57. Varga Gy, Újvári G, Kovács J, Szalai Z. Effects of particle optical properties on grain size measurements of aeolian dust deposits. *Geophys Res Abstr.* 2015;17

58. de Silva SL, Spagnuolo MG, Bridges NT, Zimbelman JR. Gravel-mantled megaripples of the Argentinian Puna: A model for their origin and growth with implications for Mars. *Geol Soc Am Bull*. 2013;**125**(11-12):1912-1929. https://doi.org/10.1130/B30916.1

59. Espinoza J, García A, Milana JP. Estructura espacial y temporal de las precipitaciones nivales en La Región de Atacama y modelación del aporte hídrico por fusión del manto nival. *XIV Congreso Geológico Chileno*. La Serena, Chile; 2015

60. Grosjean M, Veit H. Water Resources in the Arid Mountains of the Atacama Desert (Northern Chile): Past Climate Changes and Modern Conflicts. In: Huber UM, Bugmann HKM, Reasoner MA, eds. *Global Change and Mountain Regions: An Overview of Current Knowledge*. The Netherlands: Springer Netherlands; 2005: 93-104.

61. Romanovsky EV, Osterkamp ET. Effects of unfrozen water on heat and mass transport processes in the active layer and permafrost. *Permafr Periglac Process*. 2000;**11**:219-239.

62. Hanson S, Hoelzle M. The thermal regime of the active layer at the Murtèl rock glacier based on data from 2002. *Permafr Periglac Process*. 2004;**15**:273-282. https://doi.org/10.1002/ppp.499

63. Wilcox CA, Escauriaza C, Agredano R, et al. An integrated analysis of the March 2015 Atacama floods. *Geophys Res Lett.* 2016;**43**:8035-8043. https://doi.org/10.1002/2016GL069751

64. Schotterer U, Grosjean M, Stichler W, et al. Glaciers and climate in the Andes between the Equator and 30°S: What is recordedunder extreme environmental conditions? *Clim Change.* 2003;**59**:157-175. https://doi.org/10.1023/A:1024423719288

65. Ginot P, Kull C, Schotterer U, Schwikowski M, Gäggeler WH. Glacier mass balance reconstruction by sublimation induced enrichment of chemical species on Cerro Tapado (Chilean Andes). *Clim Past*. 2006;**2**:21-30. https://doi.org/10.5194/cp-2-21-2006

66. Houston J. Evaporation in the Atacama Desert: An empirical study of spatio-temporal variations and their causes. *J Hydrol*. 2006;**330**:402-412. https://doi.org/10.1016/j.jhydrol.2006.03.036

67. Zimbelman JR, Scheidt SP, de Silva SL, Bridges MG, Spagnuolo MG, Neely EM. Aerodynamic roughness height for gravel-mantled megaripples, with implications for wind profiles near TARs on Mars. *Icarus*. 2016;**266**:306-314. https://doi.org/10.1016/j.icarus.2015.11.008

68. Halloy S. Islands of life at 6000 m altitude: the environment of the highest autotrophic communities on Earth (Socompa Volcano, Andes). *Arct Antarct Alp Res.* 1991;**23**(3):247-262. https://doi.org/10.2307/1551602

69. Lawrence GP. Measurement of pore sizes in fine-textured soils: a review of existing techniques. *Eur J Soil Sci*. 1977;**28**(4):527-540. https://doi.org/10.1111/j.1365-2389.1977.tb02261.x

70. Hillel D. *Introduction to Environmental Soil Physics*. Amsterdam, The Netherlands: Elsevier Academic Press; 2003.

71. Rowel DL. *Soil science: methods and applications*. Harlow, UK: Longman Group UK Ltd; 1994.

72. Wilson RE. Humidity Control by Means of Sulfuric Acid Solutions, with Critical Compilation of Vapor Pressure Data. *J Ind Eng Chem*. 1921;**13**(4):326–331. https://doi.org/10.1021/ie50136a022

Tables

Site name	Latitude	Longitude	Elevation (m a.s.l.)	Slope (°)	Aspect	Depth (cm)	Start date	End date
Laguna Negro Francisco	27°29'16"S	69°15'23"W	4200	2.1	NE	10	Feb, 2014	Feb, 2016
						60	Feb, 2014	Feb, 2016
Murray Lodge	26°56'01"S	68°36'49"W	4550	1.2	SW	10	Feb, 2014	Feb, 2016
						35	Feb, 2014	Feb, 2016
Atacama Camp	27°04'32"S	68°33'51"W	5260	4.3	W	10	Feb, 2014	Feb, 2016
						35	Feb, 2014	Feb, 2016
						60	Feb, 2012	Feb, 2016
Tejos Camp	27°05'14"S	68°32'17"W	5830	8.1	N	10	Feb, 2012	Feb, 2016
						35	Feb, 2012	Feb, 2016
						60	Feb, 2012	Feb, 2016
Crater Edge	27°06'27"S	68°33'34"W	6750	10.3	W	10	Feb, 2012	Feb, 2016
						20	Feb, 2012	Feb, 2016
Mt. Ojos del Salado Summit	27°07'34"S	68°32'26"W	6893	1.4	E	10	Feb, 2012	Feb, 2016

Table 1. Geographical coordinates, elevation, slope and aspect – derived from SRTM V.3.0 – of our study sites, the start and end date of the ground temperature records at different depths are also shown.

	Period of analysis	Mean AMGT (C°)	Min DMGT (C°)	Max DMGT (C°)	Period of Landsat snow cover (%)	Period of Aqua snow cover (%)	Period of Terra snow cover (%)	Zero curtain period (%)
Laguna Negro Francisco (4200 m)								
Depth: 10 cm	Feb, 2014 - Feb, 2016	6.3	-7.1	18.3	44	24	21	4
Depth: 60 cm	Feb, 2014 - Feb, 2016	5.9	-4.4	15.0	44	24	21	9
Murray Lodge (4550 m)								
Depth: 10 cm	Feb, 2014 - Feb, 2016	4.8	-11.6	18.3	14	12	15	4
Depth: 35 cm	Feb, 2014 - Feb, 2016	4.8	-10.0	16.1	14	12	15	5
Atacama Camp (5260 m)								
Depth: 10 cm	Feb, 2014 - Feb, 2016	-0.7	-14.3	11.2	33	31	31	3
Depth: 35 cm	Feb, 2014 - Feb, 2016	-0.4	-12.1	9.7	34	31	32	13
Depth: 60 cm	Feb, 2012 - Feb, 2016	-0.4 ± 0.04	-7.9	6.5	23	24	25	17
Tejos Camp (5830 m)								
Depth: 10 cm	Feb/2012 - Feb/2016	-3.7 ± 0.05	-17.9	6.7	25	24	28	15
Depth: 35 cm	Feb/2012 - Feb/2016	-3.5 ± 0.13	-15.0	4.1	25	24	28	22
Depth: 60 cm	Feb/2012 - Feb/2016	-3.3 ± 0.24	-11.3	0.8	25	24	28	33
Crater Edge (6750 m)								
Depth: 10 cm	Feb, 2012 - Feb, 2016	-15.2 ± 0.5	-25.9	-4.5	85	29	45	0
Depth: 20 cm	Feb, 2012 - Feb, 2016	-14.8 ± 0.58	-22.5	-6.6	85	28	44	0
Ojos del Salado Summit (6893 m)								
Depth: 10 cm	Feb, 2012 - Feb, 2016	-17.6 ± 0.3	-32.2	-4.1	21	40	58	0

Table 2. Average values of the Annual Mean Ground Temperatures (AMGT), minimal and maximal Daily Mean Ground Temperatures (DMGT). The percentage of days characterized by zero curtains, and partial or full snow coverage – derived from Landsat, MODIS (Aqua) and MODIS (Terra) imagery – are also included.

	AT 10 cm	AT 35 cm	AT 60 cm	TE 10 cm	TE 35 cm	TE 60 cm
Particle size distribution						
Coarse fraction (% m/m)	36	18	28	54	48	60
Fine fraction (% m/m)	65	82	71	47	53	40
Silt in the fine fraction (% v/v)	6	24	18	13	30	13
Porosity						
Porosity (% v/v)	50	55	51	55	67	66
Macro- and meso-pores (% v/v)	36	46	43	33	49	47
Micro-pores (% v/v)	14	9	8	22	19	20
Density						
Bulk density (g cm^{-3})	1.3	1.5	1.5	1.1	1.3	1.0
Grain density of coarse fraction (g cm^{-3})	3.0	3.2	3.1	3.0	3.1	3.0
Grain density of fine fraction (g cm^{-3})	2.6	3.4	3.1	2.4	4.1	3.0
Hygroscopicity						
RH 96% (nm)	1081	356	277	240	165	257
RH 82% (nm)	891	296	228	202	135	219
RH 37% (nm)	450	156	121	133	85	152
RH 5.1% (nm)	67	24	18	19	12	23

Table 3. Physical properties of the regolith at different depths of the Atacama Camp (AT), 5260 m a.s.l., and the Tejos Camp (TE), 5830 m a.s.l.. Grain diameter is larger than 2 mm in the coarse fraction and smaller than 2 mm in the fine fraction, silt particles are smaller than 50 μm. The diameter of macro- and meso-pores is above 10 μm, while micro-pores are smaller than 10 μm in diameter.

Figures

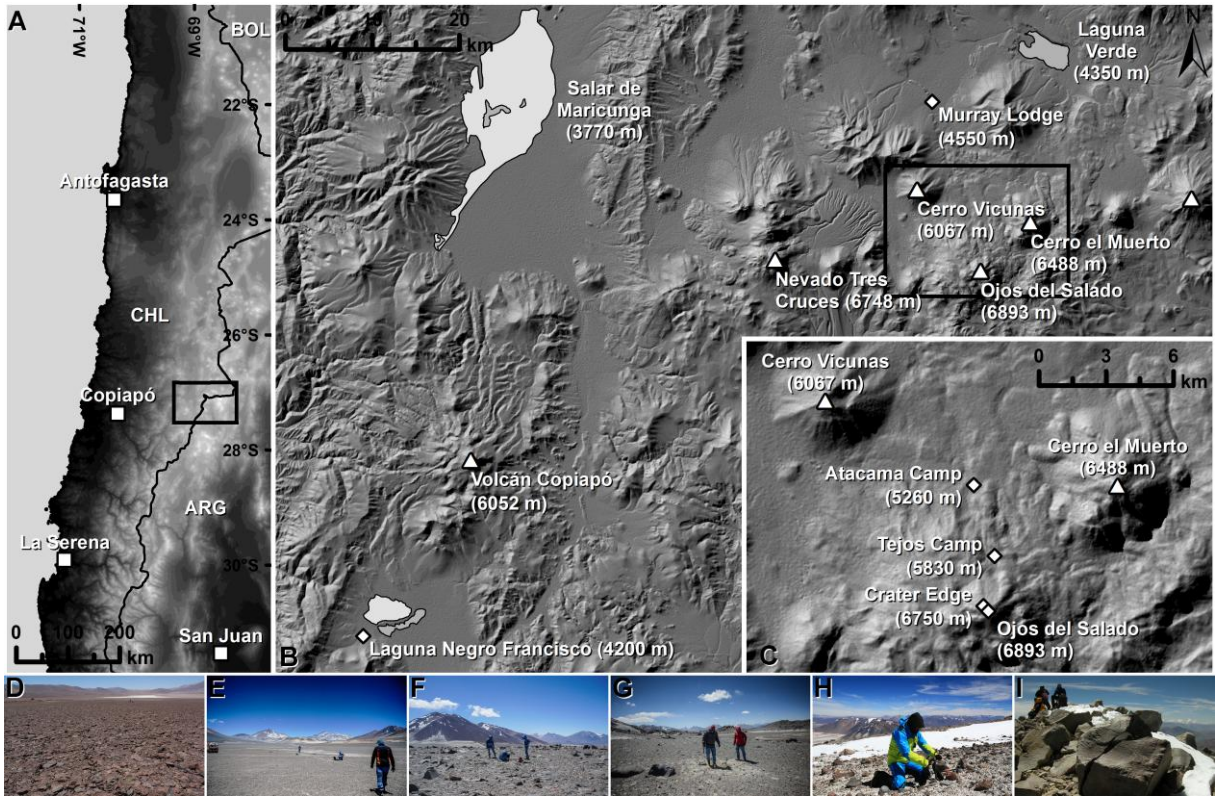

Fig 1. Our area of interest within the wider Andes (A), our study sites (white diamonds) along with major volcanic peaks (white triangles), salt lakes (dark grey polygons) and playas (light grey polygons) plotted on a Shuttle Radar Topography Mission (SRTM) V.3.0 shaded relief map (B, C). Photographs taken at the Laguna Negro Francisco (D), Murray Lodge (E), Atacama Camp (F), Tejos Camp (G), Crater Edge (H) and the Mt. Ojos del Salado summit (I).

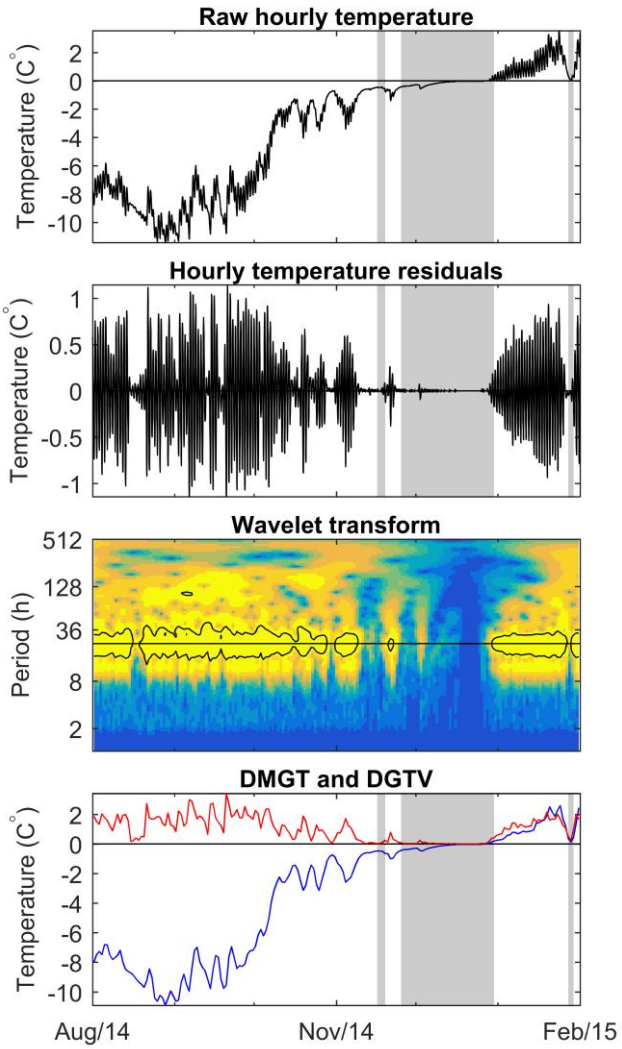

Fig 2. A sample of the raw hourly temperature record measured at the depth of 35 cm at the Tejos Camp (5830 m a.s.l.) between 01 August 2014 and 01 February 2015. The hourly temperature residuals – the centred 24 hour mean subtracted from the hourly temperature measurements – the wavelet transform of the temperature residuals and the Daily Mean Ground Temperatures (DMGT; blue solid line), Daily Ground Temperature Variations (DGTV; red solid line) are also plotted. The 0.95 confidence contour, which highlights significant temperature periodicity, is plotted on the wavelet transform panel, where the diurnal frequency axis is also highlighted. Zero curtains – delineated where the 0.95 confidence contour does not intersect the diurnal frequency axis and the raw hourly temperature is between -0.5°C and +0.5°C – are highlighted (shaded grey area) on the hourly temperature, hourly temperature residual and DMGT/DGTV panels. A distinctive zero curtain is visible during January 2015.

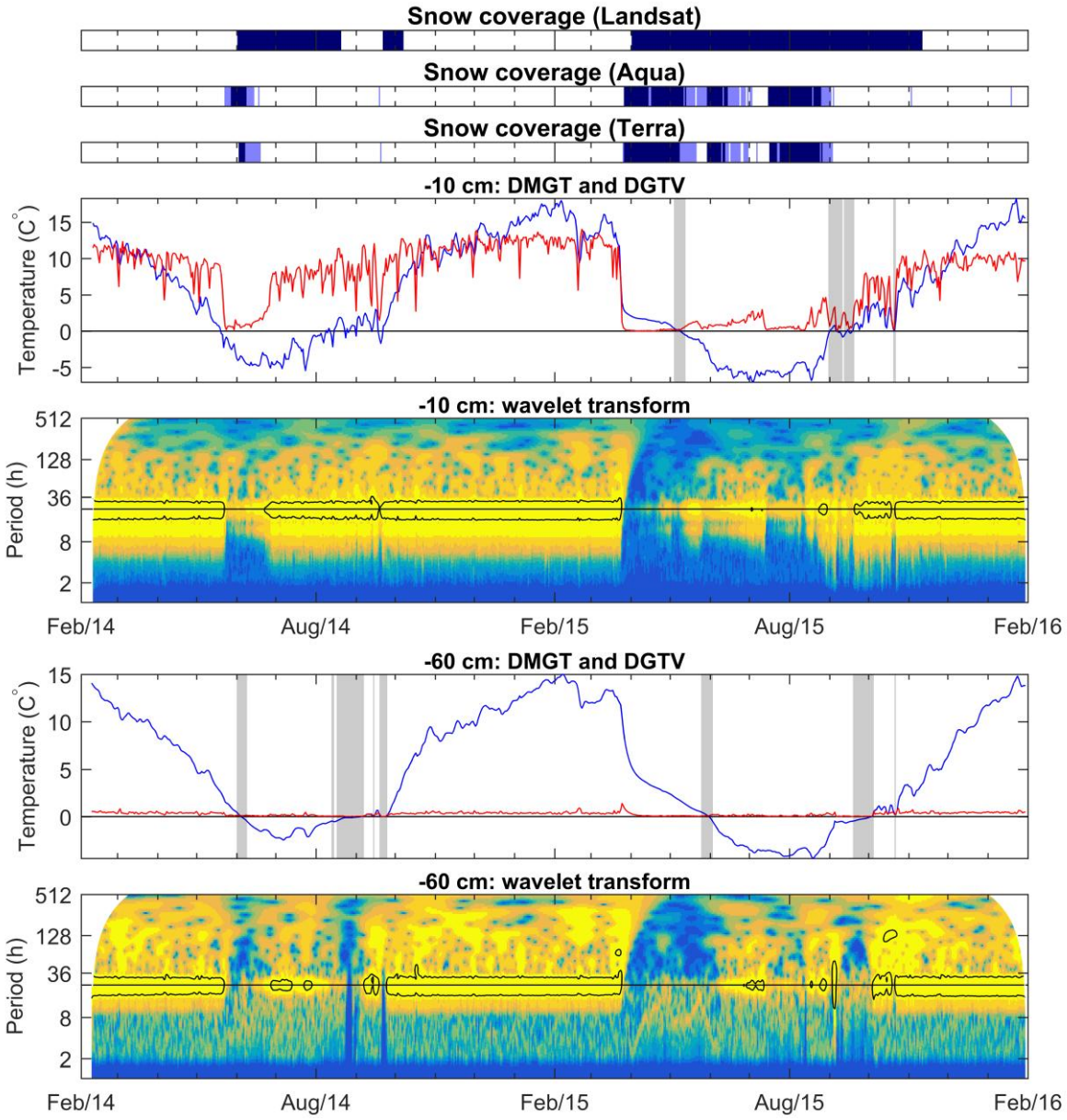

Fig 3. Snow coverage derived from Landsat, MODIS aboard Aqua and MODIS aboard Terra (light blue: partial snow coverage; dark blue: full snow coverage) at the Laguna Negro Francisco study site (4200 m a.s.l.). Daily Mean Ground Temperatures (DMGT; blue solid line), Daily Ground Temperature Variations (DGTV; red solid line) and the wavelet transform of the temperature record (yellow: strong periodicity; blue: weak periodicity) are plotted for the depths of 10 and 60 cm. The 0.95 confidence contour is plotted on the wavelet transform panels (solid black contour line), to highlight significant temperature periodicity. The diurnal frequency axis is also highlighted on the wavelet transform panels. Zero curtains are plotted (shaded gray area) on the DMGT/DGTV panels.

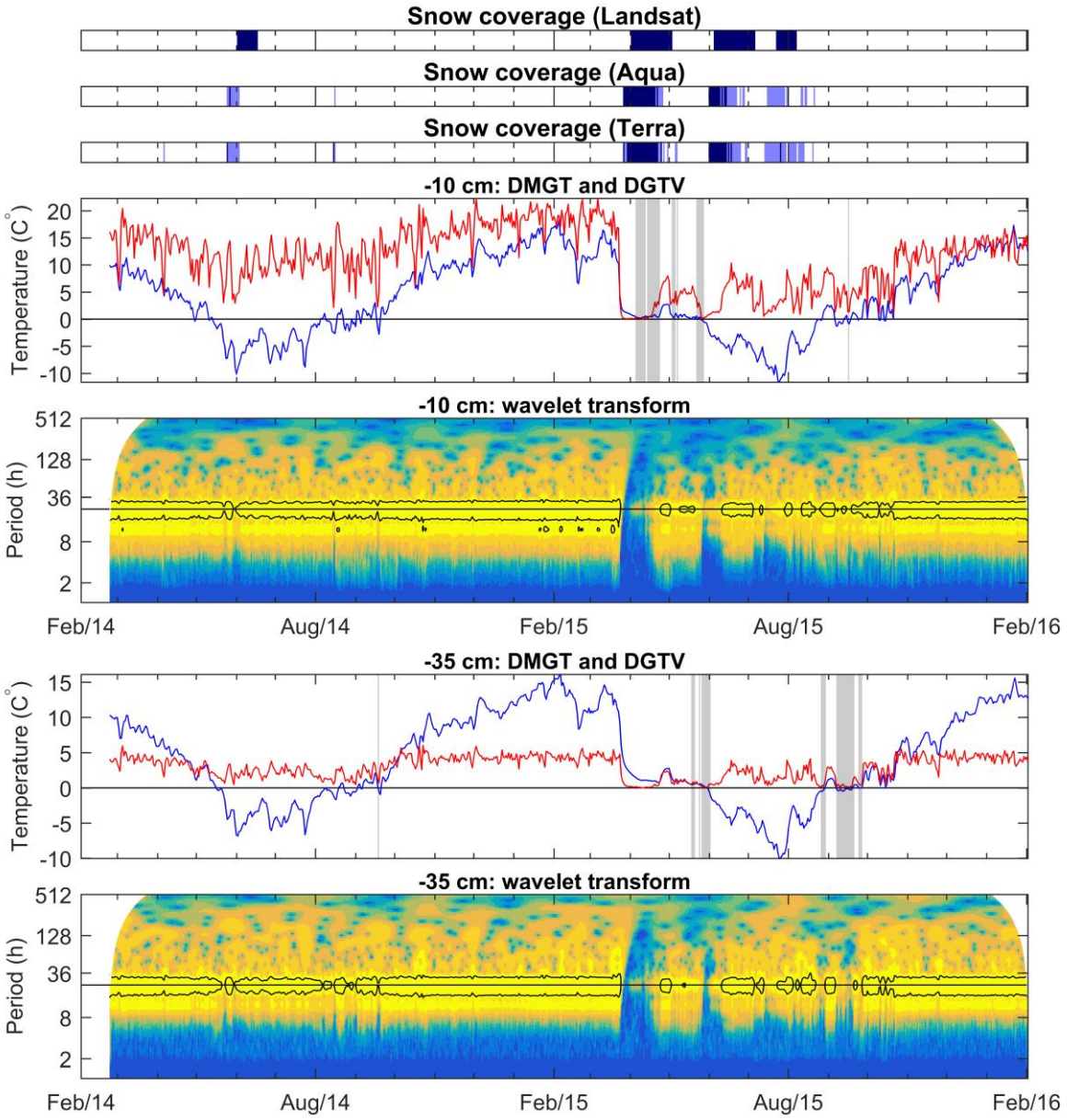

Fig 4. Results of the snow coverage and ground temperature survey – measured at the depths of 10 and 35 cm – at the Murray Lodge study site (4550 m a.s.l.). For detailed description see the caption of Figure 3.

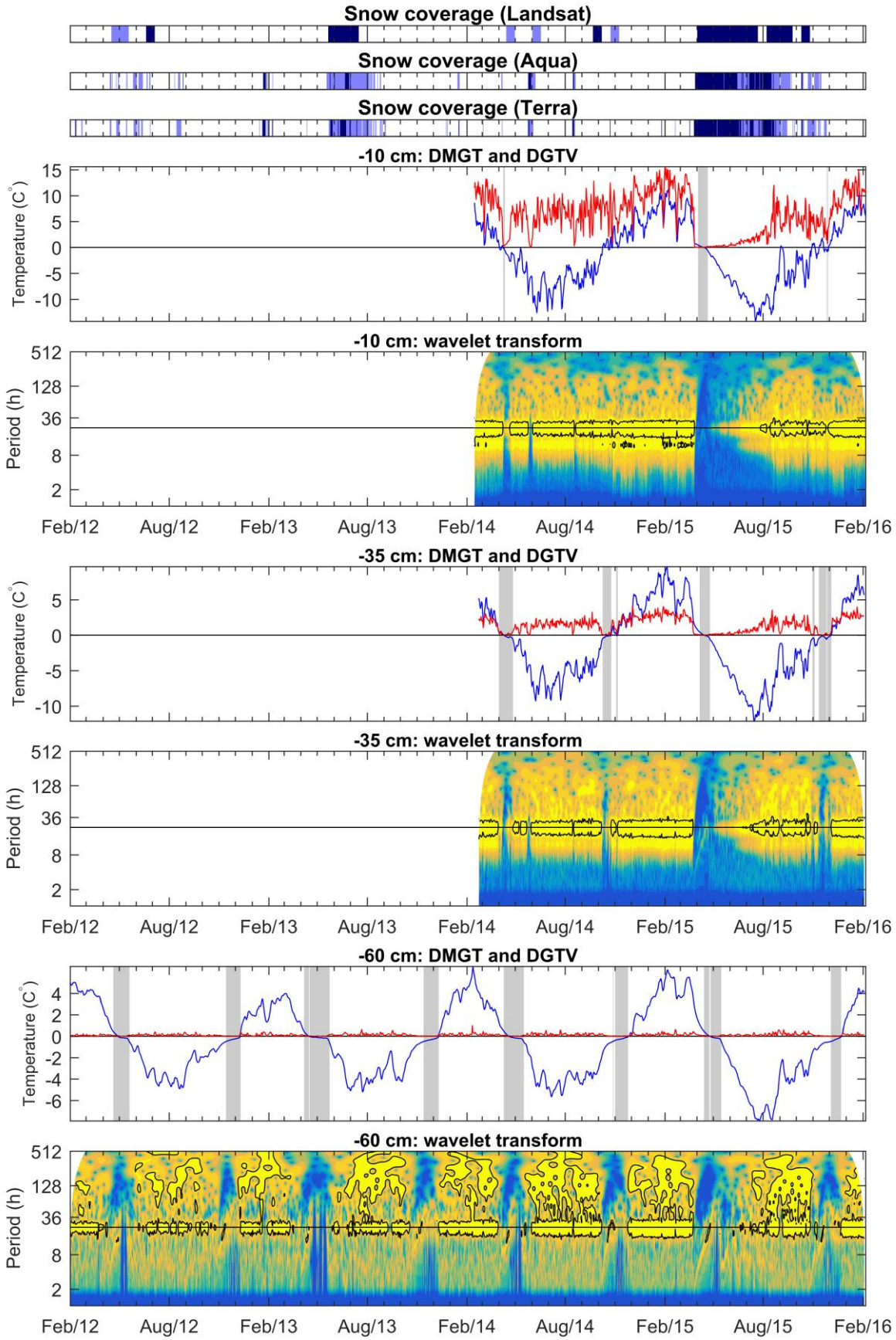

Fig 5. Results of the snow coverage and ground temperature survey – measured at the depths of 10, 35 and 60 cm – at the Atacama Camp study site (5260 m a.s.l.). For detailed description see the caption of Figure 3.

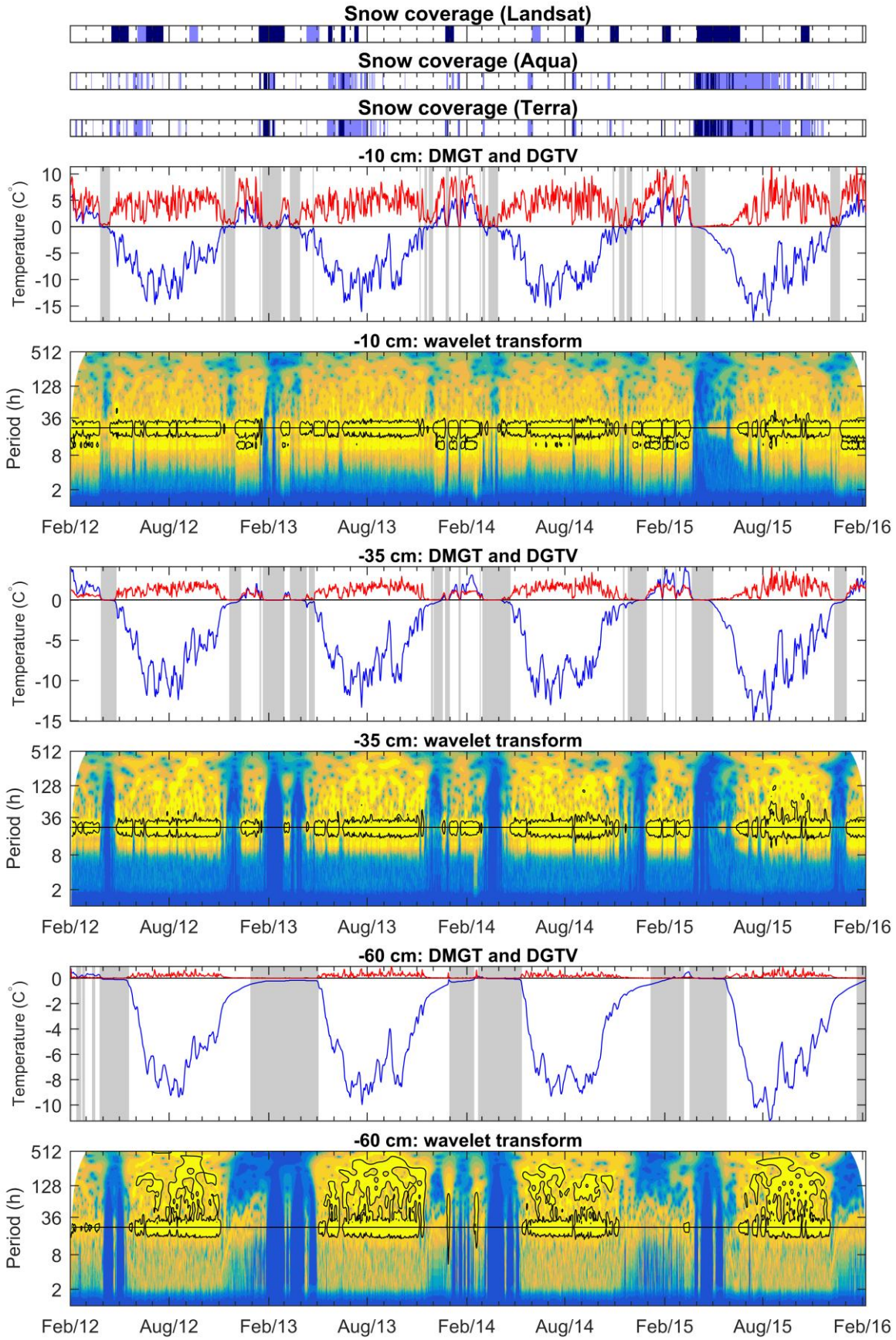

Fig 6. Results of the snow coverage and ground temperature survey – measured at the depths of 10, 35 and 60 cm – at the Tejos Camp study site (5830 m a.s.l.). For detailed description see the caption of Figure 3.

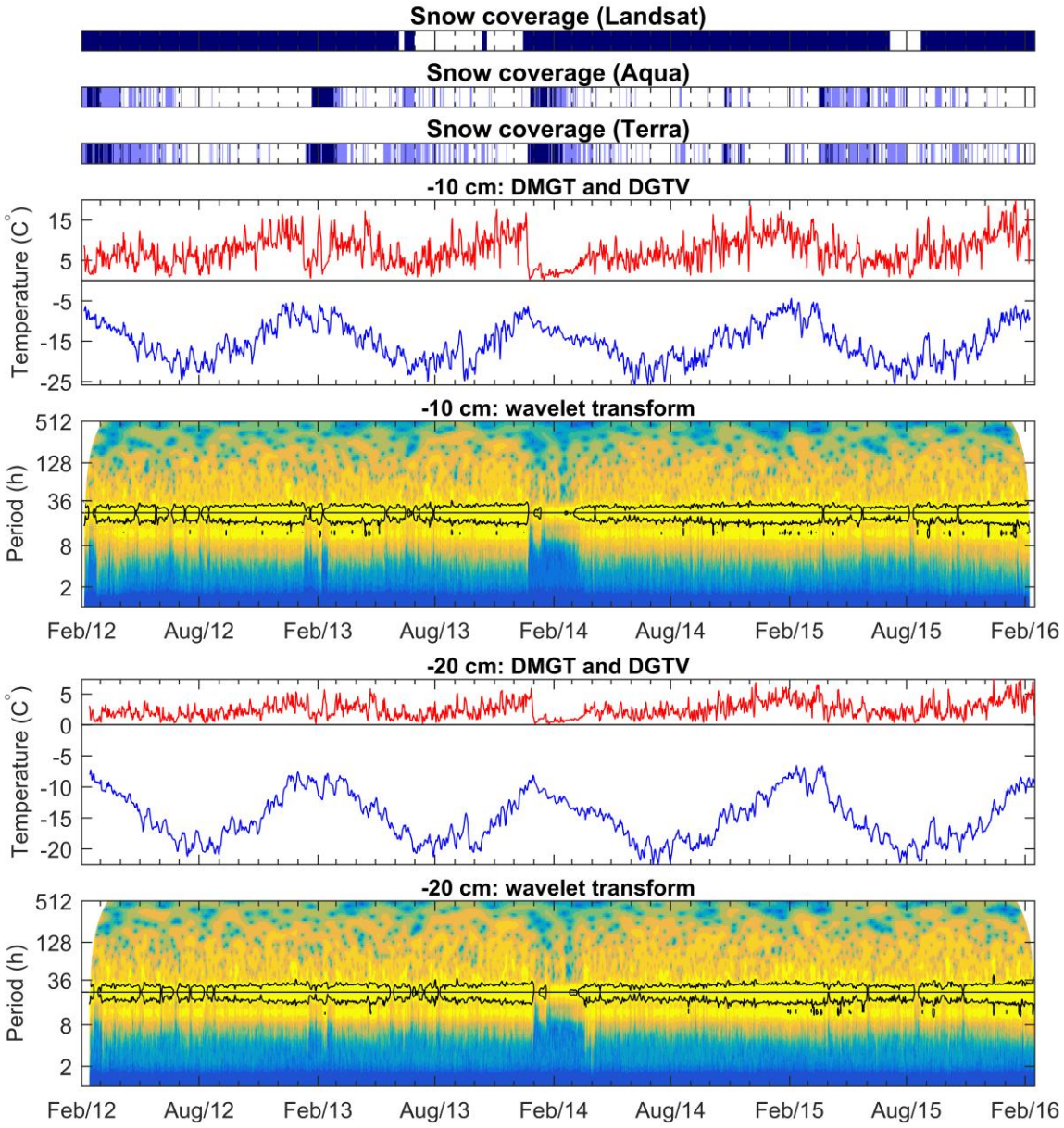

Fig 7. Results of the snow coverage and ground temperature survey – measured at the depths of 10 and 20 cm – at the Crater Edge study site (6750 m a.s.l.). For detailed description see the caption of Figure 3.

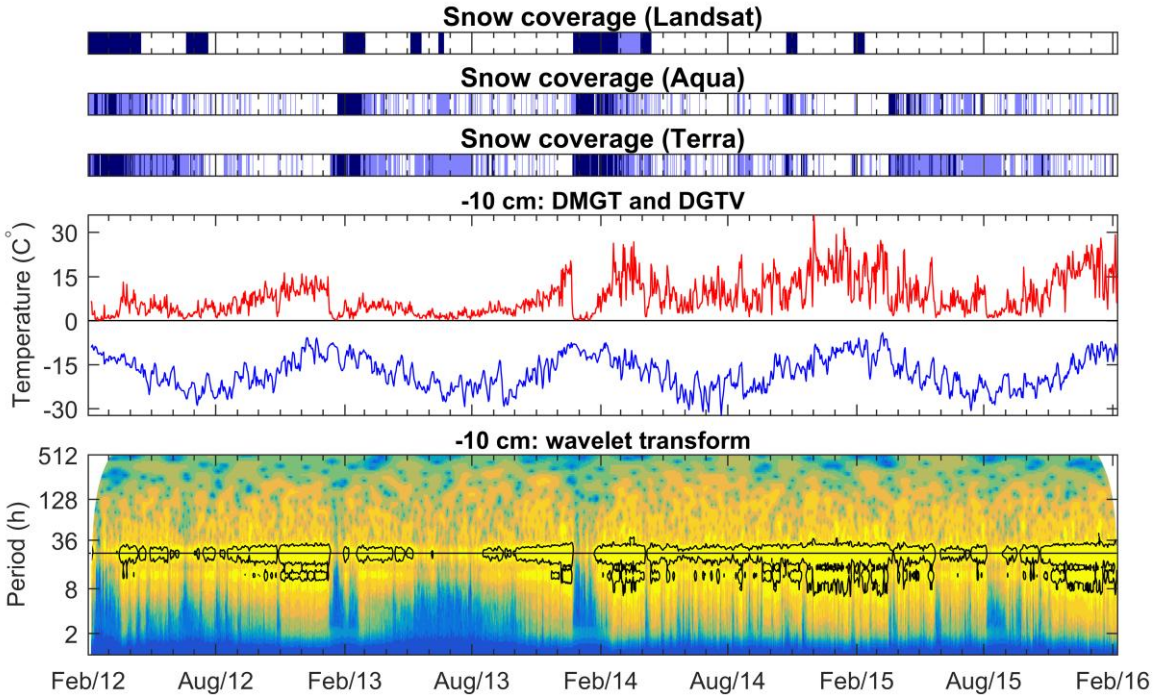

Fig 8. Results of the snow coverage and ground temperature survey – measured at the depth of 10 cm – at the Mt. Ojos del Salado summit study site (6893 m a.s.l.). For detailed description see the caption of Figure 3.

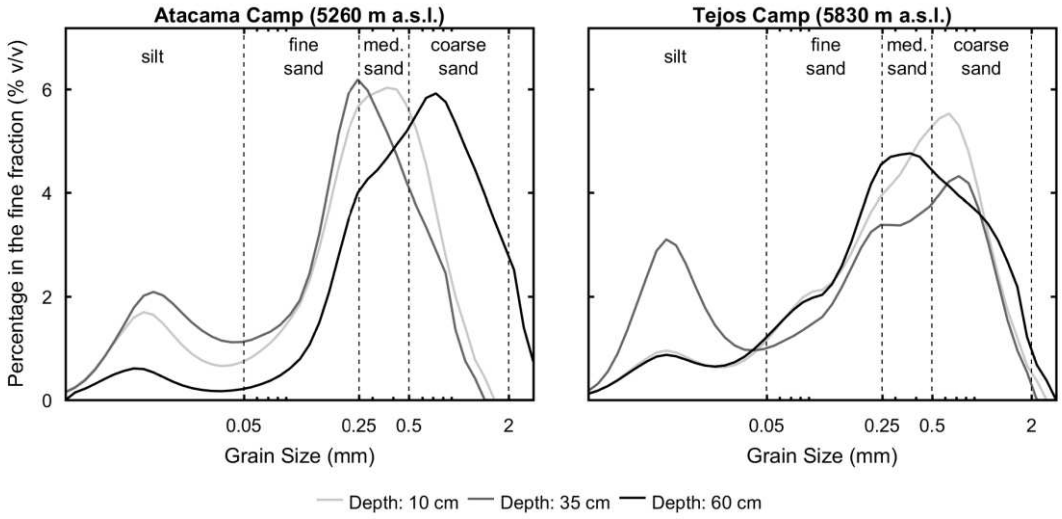

Fig 9. Particle size distribution of the fine fraction (d < 2 mm) at different depths of the Atacama Camp (5260 m a.s.l.) and the Tejos Camp (5830 m a.s.l.) study sites.

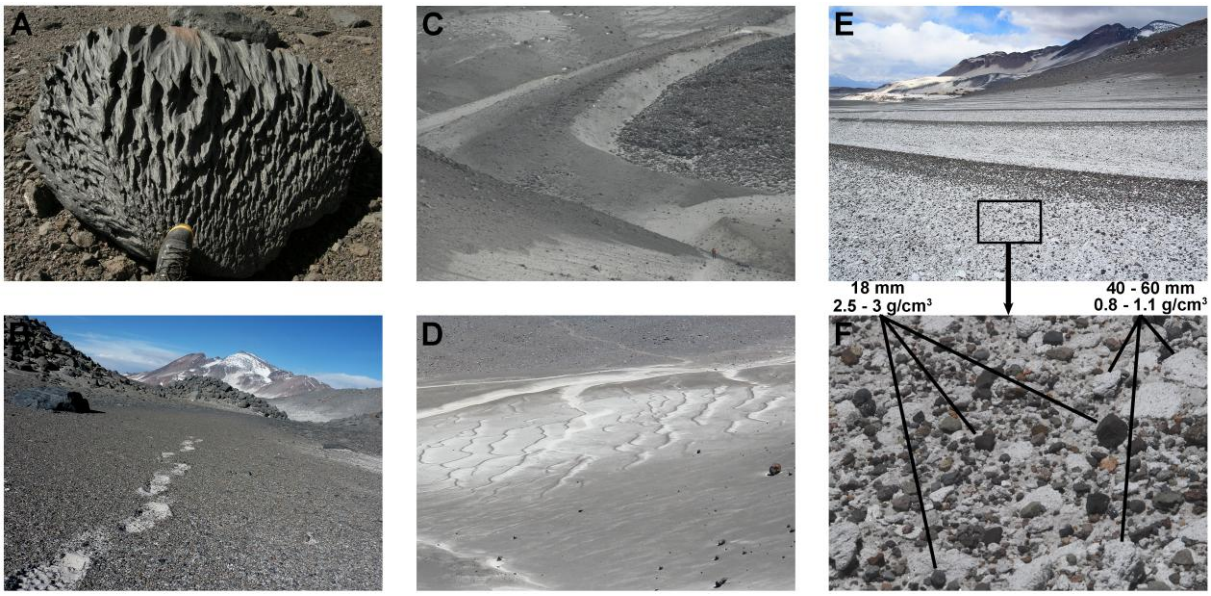

Fig 10. Aeolian landforms in the vicinity of the Atacama Camp (5260 m a.s.l.) and the Tejos Camp (5830 m a.s.l.): aggressive aeolian abrasion on the windward side of a boulder at 6000 m a.s.l. near the Tejos Camp (A), coarse lag gravel pavement between the Atacama and Tejos Camps (B), relict lateral moraine transformed into a coarse grained dune on the lee-side of an ancient lava flow between the Atacama and Tejos Camps (C), gravel-mantled megaripples next to the Atacama Camp (D and E), clasts found on a gravel-mantled megaripple (F).

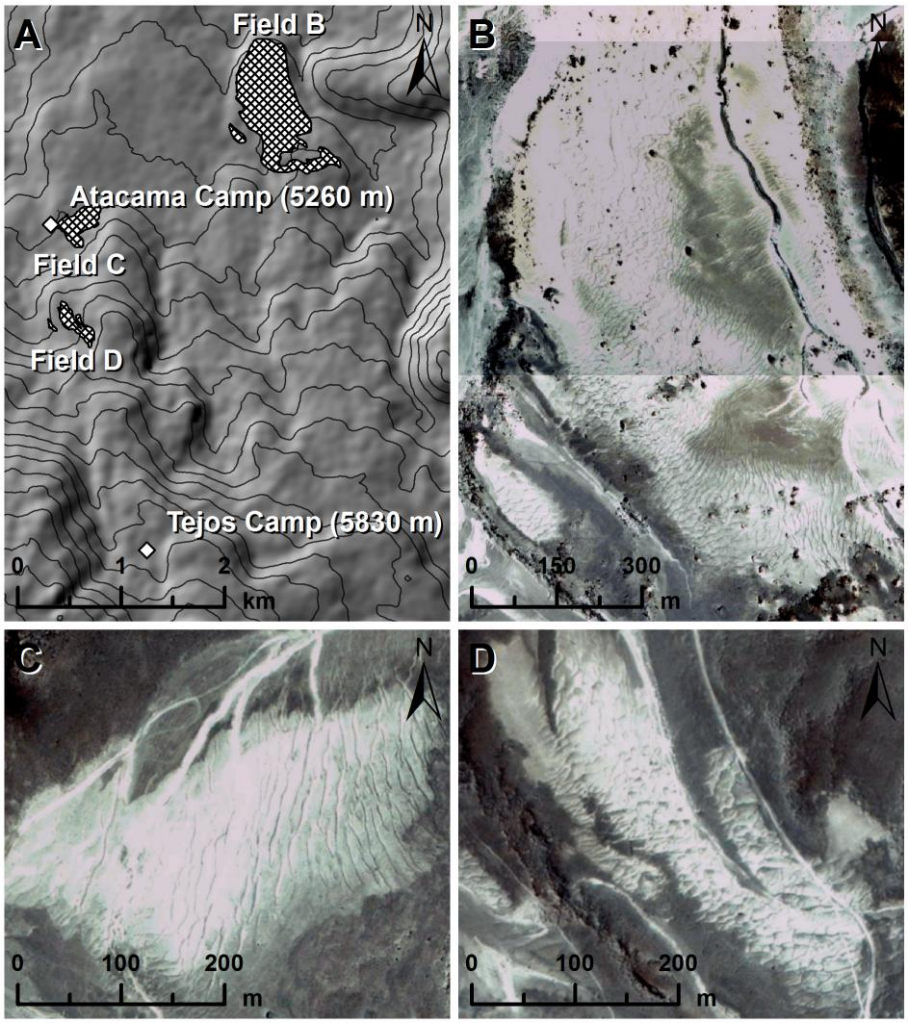

Fig 11. High altitude gravel-mantled megaripple fields in the vicinity of the Atacama Camp (5260 m a.s.l.) and the Tejos Camp (5830 m a.s.l.) plotted on an SRTM V.3.0 shaded relief map, with elevation contours at 50 m intervals (A). The three megaripple fields observed on the field are also well visible on high resolution Google Earth imagery retrieved in 2008. The fields are situated between 5140-5275 m a.s.l. (field B), 5240-5290 m a.s.l. (field C), and 5390-5480 m a.s.l. (field D) and have an area of 0.06, 0.09 and 0.63 km^2 respectively.